



Crystal structure of the HIV-1 integrase catalytic core and C-terminal domains: A model for viral DNA binding

Julian C.-H. Chen[†], Jolanta Krucinski[†], Larry J. W. Miercke[†], Janet S. Finer-Moore[†], Ann H. Tang[‡], Andrew D. Leavitt^{‡§}, and Robert M. Stroud^{†¶}

Departments of [†]Biochemistry and Biophysics, [‡]Laboratory Medicine, and [§]Internal Medicine, University of California, San Francisco, CA 94143

Communicated by David R. Davies, National Institutes of Health, Bethesda, MD, May 15, 2000 (received for review December 21, 1999)

Insolubility of full-length HIV-1 integrase (IN) limited previous structure analyses to individual domains. By introducing five point mutations, we engineered a more soluble IN that allowed us to generate multidomain HIV-1 IN crystals. The first multidomain HIV-1 IN structure is reported. It incorporates the catalytic core and C-terminal domains (residues 52–288). The structure resolved to 2.8 Å is a Y-shaped dimer. Within the dimer, the catalytic core domains form the only dimer interface, and the C-terminal domains are located 55 Å apart. A 26-aa α -helix, $\alpha 6$, links the C-terminal domain to the catalytic core. A kink in one of the two $\alpha 6$ helices occurs near a known proteolytic site, suggesting that it may act as a flexible elbow to reorient the domains during the integration process. Two proteins that bind DNA in a sequence-independent manner are structurally homologous to the HIV-1 IN C-terminal domain, suggesting a similar protein–DNA interaction in which the IN C-terminal domain may serve to bind, bend, and orient viral DNA during integration. A strip of positively charged amino acids contributed by both monomers emerges from each active site of the dimer, suggesting a minimally dimeric platform for binding each viral DNA end. The crystal structure of the isolated catalytic core domain (residues 52–210), independently determined at 1.6-Å resolution, is identical to the core domain within the two-domain 52–288 structure.

Integration of retroviral DNA into the host cell genome is required for virus replication and is mediated by viral integrase (IN) (Fig. 1). IN first removes two nucleotides from the 3' end of each strand of the nascent viral DNA, leaving a recessed 3' CA dinucleotide (3' processing). After migration into the nucleus of the infected cell as part of a nucleoprotein complex, IN covalently attaches each 3' processed viral end to the host cell DNA (strand transfer). Both 3' processing and strand transfer are divalent cation-requiring trans-esterification reactions catalyzed at a single active site in the enzyme's core (1).

Sequence alignments (2, 3), mutagenesis (4–9), and proteolytic digestion (5) suggest a three-domain structure for HIV-1 IN. The N-terminal domain, residues 1–51, contains a conserved “HH-CC” motif that binds zinc in a 1:1 stoichiometry (10). The central catalytic core domain, residues 52–210, contains the catalytic site characterized by three invariant essential acidic residues, D64, D116, and E152. The C-terminal domain, amino acids 220–288, contributes to DNA binding and oligomerization necessary for the integration process (11) and is linked to the catalytic core by residues 195–220, an extension of the final helix of the core domain.

Prior efforts to crystallize full-length HIV-1 IN have been hampered by poor solubility. The mutation F185K markedly improved solubility of the central IN catalytic core domain to over 25 mg/ml and led to its crystal structure (12, 13). Structures of the individual N-terminal (14, 15) and C-terminal domains (16–18) have been determined by NMR. Like the catalytic core domain, each isolated terminal domain dimerizes in solution. Multidomain structures would provide insight into the relative spatial arrangement of the three domains, how IN binds to the

host DNA and the viral DNA ends (*att* sites) during the 3' processing and strand transfer reactions, and the oligomeric state of the active enzyme. To address these questions, we sought first to develop a more soluble form of functional, full-length IN (IN^{1–288}) for crystallization.

The introduction of five point mutations, C56S, W131D, F139D, F185K, and C280S, improved the solubility of full-length IN^{1–288} and allowed for its crystallization. To date, however, IN^{1–288} crystals have diffracted to 8-Å resolution. Truncations of the penta-mutated IN^{1–288} yielded a 2.8-Å resolution crystal structure of a two-domain construct involving the catalytic core and the C-terminal domains (IN^{52–288}) and a 1.6-Å resolution crystal structure of the catalytic core domain (IN^{52–210}) as reported here.

Materials and Methods

Mutagenesis. Mutations C56S, W131D, F139D, F185K, and C280S were introduced into a synthetic full-length HIV-1 IN (SF1) sequence in a pT7–7 vector by using oligonucleotide mutagenesis. An N-terminal 6-histidine (6-His) tag followed by a thrombin cleavage site (Stratagene) was added to facilitate purification. One- and two-domain truncation constructs, IN^{52–210} and IN^{52–288}, were generated from the penta-mutated IN^{1–288}. All mutations, the 6-His tag, and the thrombin cleavage site were confirmed by DNA sequencing.

IN Expression and Purification. The 6-His-tagged IN^{52–288} was expressed in BL21 cells by using the pT7–7 isopropyl β -D-thiogalactoside-inducible promoter. After sonication and dounce lysis, the protein was purified by using a Ni²⁺ column (Qiagen, Chatsworth, CA). After thrombin (Novagen) cleavage, thrombin was removed by passage over a benzamidine column (Amersham Pharmacia). The cleaved 6-His tag and any uncleaved protein were removed by passage over a Ni²⁺ column. Purified IN^{52–288} migrated as a single band on SDS/PAGE. Identical methods were used to purify IN^{52–210}. Purified protein was filtered (0.8/0.2 μ m syringe filter; Gelman), concentrated by high-pressure, stirred-cell ultrafiltration (YM-10 membrane; Amicon), and dialyzed against 10 mM Hepes (pH 7.0), 500 mM NaCl, and 3 mM DTT. The final protein concentration ranged from 8 to 12 mg/ml or 6 to 10 mg/ml as determined by Bradford assay using a BSA standard or absorption at 280 nm with a

Abbreviations: IN, integrase; CHAPS, 3-[(3-cholamidopropyl)dimethylammonio]-1-propanesulfonate; SIV, simian immunodeficiency virus; RSV, Rous sarcoma virus; SH3, Src homology 3.

Data deposition: The atomic coordinates have been deposited in the Protein Data Bank, www.rcsb.org [PDB ID codes 1EXQ (IN^{52–210}) and 1EX4 (IN^{52–288})].

[¶]To whom reprint requests should be addressed. E-mail: stroud@msg.ucsf.edu.

The publication costs of this article were defrayed in part by page charge payment. This article must therefore be hereby marked “advertisement” in accordance with 18 U.S.C. §1734 solely to indicate this fact.

Article published online before print: *Proc. Natl. Acad. Sci. USA*, 10.1073/pnas.150220297. Article and publication date are at www.pnas.org/cgi/doi/10.1073/pnas.150220297

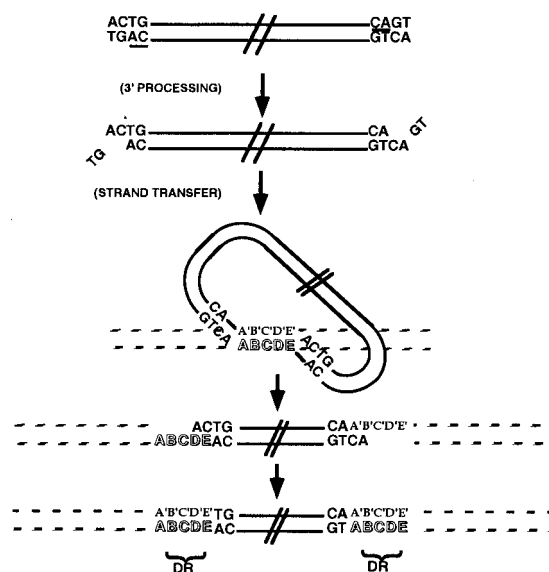


Fig. 1. HIV-1 IN activities. A schematic diagram of HIV-1 IN activities depicts the double-stranded DNA viral genome at the top as parallel black lines with the terminal nucleotides CAGT. The conserved 3' CA dinucleotide is underlined at each viral end. IN first acts in the cytoplasm to remove the two 3' nucleotides (3' processing), leaving a 2-nt overhang at each 5' end. In the nucleus, IN mediates a concerted integration (strand transfer) by ligating each 3' end of the viral DNA (looped structure) to the host DNA (striped lines). This generates a "gapped intermediate" with free viral 5' ends that are repaired to generate the fully integrated provirus. The characteristic HIV-1 5-bp staggered strand transfer is depicted by the letters A-E in the target DNA, and the resulting 5-bp direct repeats (DR) of host DNA flanking the provirus are indicated.

calculated extinction coefficient of 37,930 liter/mol·cm and calculated mass of 28,022 g/mol, respectively.

Crystallization. Crystals were grown in hanging drops at room temperature by vapor diffusion. Well buffer for IN⁵²⁻²⁸⁸ was 2.2 M Na formate, 150 mM Na citrate, 3 mM DTT, 3 mM 3-[(3-cholamidopropyl)dimethylammonio]-1-propanesulfonate (CHAPS), pH 5.6. Well buffer for IN⁵²⁻²¹⁰ was 1.7 M ammonium sulfate, 50 mM CdCl₂, 150 mM Na citrate, 5 mM DTT, pH 5.6. Drops were made by mixing 4 μl of purified protein solution with 4 μl of well buffer. To decrease the equilibration rate, a 1:1 mixture of paraffin and silicon oils (Hampton Research, Riverside, CA) was applied over the well solution. Trigonal IN⁵²⁻²⁸⁸ crystals, 350 × 250 × 100 μm, grew over several weeks. Bipyramidal IN⁵²⁻²¹⁰ crystals typically grew to ≈400 μm in each dimension. Before data collection, crystals were transferred to a cryoprotectant consisting of well buffer containing 15% (vol/vol) sucrose (IN⁵²⁻²¹⁰) or 20% (vol/vol) glycerol (IN⁵²⁻²⁸⁸) and frozen in a 90 K nitrogen gas stream.

Structure Determination. Diffraction was recorded by using a Mar Research image plate detector at the Stanford Synchrotron Radiation Laboratory. Intensities were integrated and scaled by using DENZO/SCALEPACK (19). The structure of the core alone, IN⁵²⁻²¹⁰, was solved by molecular replacement applied in CNS (20) by using the IN (F185K) catalytic core (21) as a search model (Protein Data Bank code 1bis). The rotation function yielded a clear solution, which gave an unambiguous translation solution. Difference Fourier refinement (22) and manual rebuilding using CHAIN (23) were interspersed with positional, *B* factor, and simulated annealing protocols in CNS to define the structure.

The structure of two-domain IN⁵²⁻²⁸⁸ was solved first by

location of the catalytic core dimer by molecular replacement, as implemented in CNS with the 1.6-Å catalytic core structure as a search model. A clear rotation solution was found (top product correlation peak 0.0410, next highest 0.0384), and this top peak also gave the highest translation solution (0.247, next highest 0.157). This initial placement gave a R_{cryst} of 53.7%. $2F_o - F_c$ maps, and $F_o - F_c$ difference maps phased on the core dimer alone revealed additional density for the C-terminal domains, confirming the correctness of the solution.

The initial interpretation of the C-terminal domains of IN⁵²⁻²⁸⁸ was facilitated by placement of the averaged NMR structure of the IN²²⁰⁻²⁷⁰ monomer (Protein Data Bank code 1ihw) (17) into the density maps using EPMR (24). These domains were located with correlation coefficients of 0.41 (next highest 0.39), and 0.44 (next highest 0.41). The solution clarified the helical linkages between the catalytic core and C-terminal domains. The initial R_{cryst} for the catalytic core domain dimer plus the two C-terminal domains, the dimeric IN⁵²⁻²⁸⁸ structure, was 48.7%.

The IN⁵²⁻²⁸⁸ structure was refined by using rigid body, positional, *B* factor, and simulated annealing protocols in CNS. Parallel refinements run with and without NCS restraints gave lower R_{cryst} and R_{free} values without restraints, suggesting that the two monomers had different microstructures determined by their different environments. NCS restraints were therefore not applied.

Results

Mutagenesis to Increase IN Solubility. In addition to the previously described F185K mutation (12, 13), we introduced mutations W131D and F139D to eliminate two hydrophobic residues on the core surface (12) and mutations C56S and C280S to minimize oxidation (25). This penta-mutated, full-length IN, IN¹⁻²⁸⁸, remains in solution at > 12 mg/ml for over 30 days. It can perform 3' processing and strand transfer activities and yields reproducible crystals. However, the IN¹⁻²⁸⁸ crystals diffract to 8 Å. Truncations of the mutated IN¹⁻²⁸⁸ yielded single- and two-domain constructs, IN⁵²⁻²¹⁰ and IN⁵²⁻²⁸⁸, each of which formed crystals that diffracted to high and intermediate resolution, respectively.

Structure of the HIV-1 IN Core Domain. Crystals of the isolated catalytic core domain, IN⁵²⁻²¹⁰, grew in a previously uncharacterized crystal form (space group P3₂, $a = 48.9$, $c = 103.6$ Å, one dimer/asymmetric unit) and diffracted beyond 1.6-Å resolution. This structure was solved by molecular replacement and refined to a R_{cryst} of 25.2%, R_{free} of 26.9% for all reflections to 1.6 Å (Table 1). The structure has the same α - β fold and dimer interface as seen in previous structures of the catalytic core domain of HIV-1 IN (12, 13, 21, 26, 27), simian immunodeficiency virus (SIV) IN (28), and Rous sarcoma virus (RSV) IN (29). The mutations introduced to improve IN solubility therefore did not change the catalytic core domain crystal structure.

Two-Domain HIV-1 IN Structure. Two-domain IN⁵²⁻²⁸⁸ crystals diffracted to 2.8-Å resolution (space group P312, $a = 104.0$, $c = 101.4$ Å, with one dimer/asymmetric unit) (Table 1). The catalytic core domain within IN⁵²⁻²⁸⁸ forms a symmetric dimer that is very similar to the crystal structure of the isolated catalytic core domain, IN⁵²⁻²¹⁰ ($C\alpha$ rms deviation of 0.6 Å between monomers) (30). Each catalytic core domain of the IN⁵²⁻²⁸⁸ dimer is linked to the C-terminal domain by residues 195–220 of helix $\alpha 6$. The divergent orientation of the two linking $\alpha 6$ helices within the dimer places the centers of the C-terminal domains ≈55 Å apart within the dimer, imparting a "Y" shape to the IN⁵²⁻²⁸⁸ structure (Fig. 2 *a* and *b*). However, the orientations of the two C-terminal domains differ by ≈90° with respect to their 2-fold-related positions, gauged by using the 2-fold axis of the

Table 1. Data collection and refinement statistics

Structure	IN ⁵²⁻²¹⁰	IN ⁵²⁻²⁸⁸
Source	SSRL 7-1 ($\lambda = 1.08 \text{ \AA}$)	SSRL 9-1 ($\lambda = 0.98 \text{ \AA}$)
Resolution, \AA	30-1.6	30-2.8
Space group	P3 ₂	P312
Unit cell, \AA	$a = 48.89, c = 103.64$	$a = 103.99, c = 101.38$
Measured reflections	213,312	178,921
Independent reflections	35,602	15,580
Completeness, %	97.3	99.8
$\langle I/\sigma(I) \rangle$	17.0	22.1
$R_{\text{merge}}, \%^*$	5.3	7.7
Wilson $\langle B \rangle, \text{\AA}^2$	24	68
$\langle B \rangle, \text{\AA}^2$	30	73
$R_{\text{free}} (\%) (F > 3\sigma)$	26.9 (24.8)	30.8 (28.4)
$R_{\text{cryst}} (\%) (F > 3\sigma)$	25.2 (22.8)	26.0 (24.3)
rmsd bond angles, deg	1.1	1.6
rmsd bond lengths, \AA	0.005	0.007
Luzzati error, \AA	0.25	0.44
Ramachandran distribution		
Most favored, %	89.1	81.5
Allowed, %	10.9	18.5
Waters	99	81

rmsd, rms deviation.

* $R_{\text{merge}} = \sum |I - \langle I \rangle| / \sum \langle I \rangle$; negative intensities included as zero.

catalytic core domain (Fig. 2). An electrostatic potential map identifies a contiguous strip of positive charge along the outer face of the IN⁵²⁻²⁸⁸ dimer, beginning at the active site of one monomer and extending along the linking $\alpha 6$ helix of the other monomer (Fig. 3a).

All residues from position 56–137, 150–185, and 195–212 of the catalytic core domain within IN⁵²⁻²⁸⁸ were clearly defined in conformation in both monomers. Residues 138–149 in the active site region, and residues 186–194 between the $\alpha 5$ and $\alpha 6$ helices, are flexible loops in poorly defined density, as previously noted in other unliganded core domain structures (12, 26, 31). However, residues 138–141 and 145–149 could be interpreted in monomer A, and the 186–194 loop in both monomers could be built into weak density based on its location in the 1.6- \AA resolution IN⁵²⁻²¹⁰ structure. Residues 210–270 containing linking helix $\alpha 6$ and the C-terminal domain were ordered in both monomers of the IN⁵²⁻²⁸⁸ dimer. Residues 271–288 are not clearly defined in density maps.

The average B factor of the catalytic core domain atoms within IN⁵²⁻²⁸⁸ is 85 \AA^2 , much higher than the 33 \AA^2 seen in the 1.6- \AA IN⁵²⁻²¹⁰ structure of the isolated catalytic core domain. In contrast, the C-terminal domains of IN⁵²⁻²⁸⁸, which form nearly all of the dimer-dimer crystal contacts, have an average B factor of 47 \AA^2 . The average B factor of 85 \AA^2 for the core implies an average amplitude of thermal vibration of $u = 1.04 \text{ \AA}$ ($B = 8 \pi^2 \langle u^2 \rangle$). To investigate how well the structure of the high B factor core domain is defined by the density map, a simulated annealing composite omit map was constructed. This was done by leaving out the structure within sequential volumes of the structure throughout the asymmetric unit, and then refining the remainder of the structure by simulated annealing. Omit maps for each “omitted” volume were calculated and reassembled into a composite omit map (Fig. 4a). It revealed continuous density for the backbone and essentially all of the side chains (Fig. 4a), showing that the high B factor core domain is clearly defined when in the context of this lower B factor C-terminal domain. The source of the higher B factors is suggested by the fact that there is only one very small crystal contact involving the core. The B factors also generally increase with distance from the C-terminal tethering $\alpha 6$ helix, implying a rigid body libration of the otherwise well-ordered core domains.

Folds of β -sheets within individual C-terminal domains of IN⁵²⁻²⁸⁸, composed of residues 223–228 ($\beta 1$), 235–245 ($\beta 2$), 248–252 ($\beta 3$), 256–260 ($\beta 4$), and 265–268 ($\beta 5$), are similar to the solution NMR structure for the isolated HIV-1 IN C-terminal domain (18). The C-terminal domain is a sandwich of two three-stranded antiparallel β -sheets. The two three-stranded antiparallel β -sheets are formed by a noncontiguous triad of strands $\beta 1$ – $\beta 2$ – $\beta 5$ (involving the N-terminal end of $\beta 2$) and a contiguous triad of strands $\beta 2$ – $\beta 3$ – $\beta 4$ (involving the C-terminal end of $\beta 2$). The longer $\beta 2$ strand transitions between the two sheets and is interrupted between sheets by a cis-proline, P238 (Fig. 4b).

C-Terminal Domain Interactions of IN⁵²⁻²⁸⁸. The vast majority of dimer-dimer contacts in the IN⁵²⁻²⁸⁸ crystal structure are mediated by C-terminal domain interactions involving four adjacent dimers that meet around a crystallographic 2-fold axis to form four different types of contacts, interfaces B, B', C, and D (Fig. 5). Interfaces B and B' involve packing of the $\beta 2$ – $\beta 3$ – $\beta 4$ sheet against the same $\beta 2$ – $\beta 3$ – $\beta 4$ sheet of a 2-fold related molecule in a parallel manner (Fig. 5). However, a CHAPS molecule wedged between the two sheets, and in contact with L242 and W243, mediates this packing of hydrophobic surfaces. In addition to the

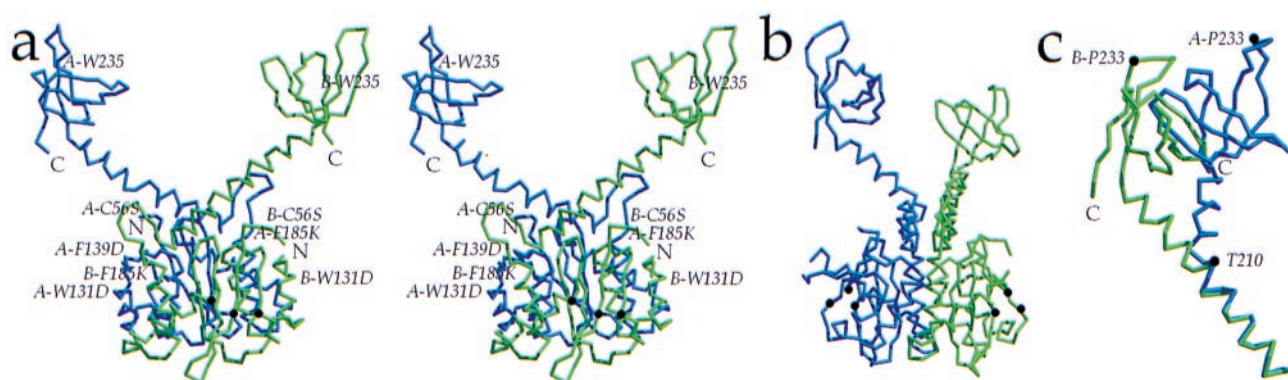


Fig. 2. Structure of HIV-1 IN⁵²⁻²⁸⁸. (a) Stereoview of the HIV-1 IN⁵²⁻²⁸⁸ dimer, composed of monomer A (blue) and monomer B (green). Monomer B catalytic residues D64, D116, and E152 are indicated (brown dots), and the N and C termini of each monomer are labeled. Immunologically critical residue W235 is located on the surface. Mutated residues C56S, W131D, F139D, and F185K are indicated, except for C280S, which is disordered. (b) The HIV-1 IN⁵²⁻²⁸⁸ dimer rotated by 90° with respect to a. Catalytic residues are highlighted in brown. (c) Alignment of residues 195–210 in $\alpha 6$ demonstrates the kink at T210 that creates a $\approx 90^\circ$ rotation of the C-terminal domains relative to one another as illustrated by the position of P233. Figure was generated by MOLSCRIPT (44) and RASTER3D (45).

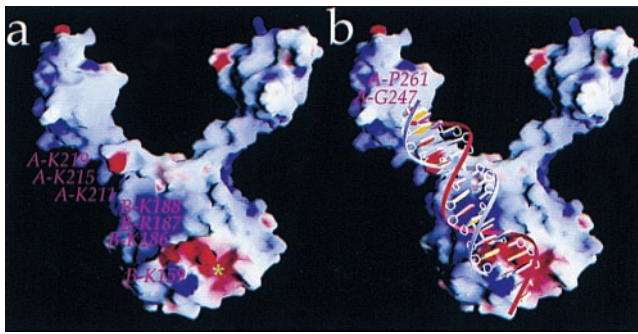


Fig. 3. Electrostatic potential map of the HIV-1 IN⁵²⁻²⁸⁸ dimer. (a) The dimer orientation is the same as in Fig. 2a. Potentials range from $-15/kT$ (red) to $+15/kT$ (blue). The strip of positive charge (blue) coursing up and to the left contains residues from both monomers of the dimer, K211, K215, and K219 from monomer A and K159, K186, R187, K188 from monomer B. The active site pocket of monomer B (*) includes catalytic residues D64, D116, and E152. (b) An 18-bp viral DNA end is modeled onto the IN dimer with the positively charged residues in contact with the DNA phosphodiester backbone. The adenine base of the conserved viral 3' CA dinucleotide contacts K159. Docking of DNA was done with MIDAS (46). Figure was generated by GRASP (47).

CHAPS-mediated interactions at this interface, hydrogen bonding and hydrophobic interactions occur between the $\beta 2$ - $\beta 3$ - $\beta 4$ sheet and linking helix $\alpha 6$ from the 2-fold-related molecule (Fig. 5b). Because of the kink in the linking $\alpha 6$ helix, interface B' possesses a greater number of interactions between the $\beta 2$ - $\beta 3$ - $\beta 4$ sheet and linking helix $\alpha 6$ than does interface B. Interface C involves the antiparallel packing of the noncontiguous $\beta 1$ - $\beta 2$ - $\beta 5$ sheets from different dimers against each other (Fig. 5b). Again, a CHAPS molecule is wedged in between these hydrophobic surfaces, and the only direct contact between sheets is a hydrogen bond between R224N η 1 and the carbonyl oxygen of W235. Interface D does not lie across a symmetry axis and is formed by edge-to-edge association of the $\beta 2$ - $\beta 3$ loop 242-246 against the $\beta 5$ strand 265-269 of the symmetry-related molecule (Fig. 5b).

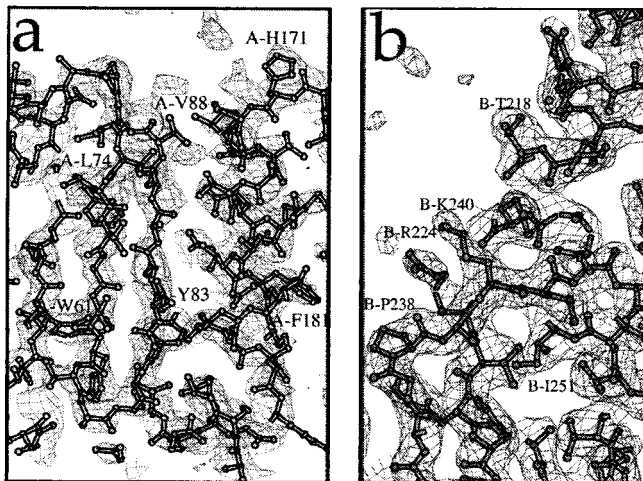


Fig. 4. Electron density plots from the IN⁵²⁻²⁸⁸ structure. (a) Plot of a simulated annealing composite omit map showing $2F_o - F_c$ density contoured at 1σ in a region of the HIV-1 IN⁵²⁻²⁸⁸ catalytic core domain. The refined structure is superimposed on the density plot. (b) Plot of a $2F_o - F_c$ map, contoured at 1.2σ , around linking helix $\alpha 6$ and the C-terminal domain of monomer B. At the left is the cis-proline, P238, where $\beta 2$ sharply changes direction and transitions between the two β -sheets within the C-terminal domain. Maps were generated by CNS (20). Figure was generated by MOLSCRIPT (44) and locally written FRODO MOL.

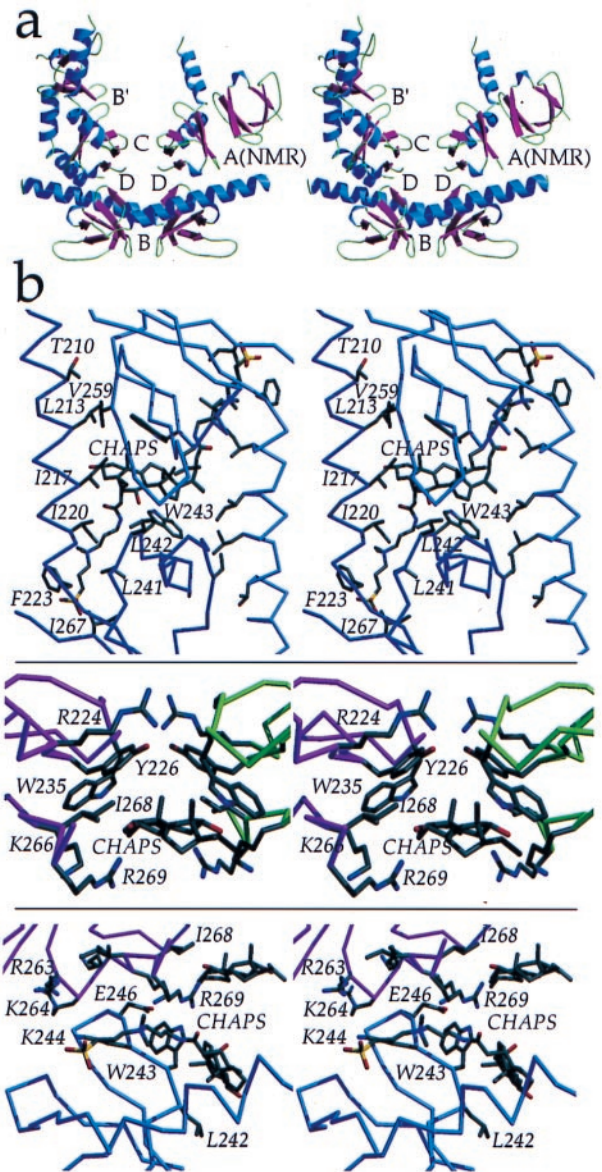


Fig. 5. SH3-SH3 interactions. (a) The C-terminal domains within the IN⁵²⁻²⁸⁸ dimer are 55 Å apart, but four different dimer-dimer contacts involving interactions between adjacent C-terminal domains, interfaces B, B', C, and D, are found within the crystal. All four of these interfaces differ from interface A, which is found in the NMR structure of isolated C-terminal domains. Buried molecular surface areas for the interfaces are: B = 1,695 Å² (2), B' = 2,589 Å² (2), C = 697 Å² (2), D = 764 Å² (2), and A(NMR) = 660 Å² (2). β -strands (magenta), α -helices (blue), and loops (green) are color coded. (b) Interactions between adjacent C-terminal domains and protein-detergent (CHAPS) interactions are shown. (Top) Interface B, in an orientation rotated 90° relative to that in a. (Middle) Interface C. (Bottom) Interface D. Interfaces C and D are in an identical orientation as in a. Figure was generated by using MOLSCRIPT (44) and RASTER3D (45). Surface area was calculated by using SURFACE (48).

Discussion

The Y-shaped dimer of HIV-1 IN⁵²⁻²⁸⁸ to 2.8-Å resolution is the first reported multidomain structure for HIV-1 IN and can be compared with analogous structures for RSV IN (32) and SIV IN (28). The introduction of five mutations, C56S, W131D, F139D, F185K, and C280S, did not alter the structure of the catalytic core compared with other structures containing only one of these four mutations, F185K (12), or mutation F185H (26, 31). The finding of an identical catalytic core domain structure

alone (IN⁵²⁻²¹⁰) or attached to the C-terminal domain (IN⁵²⁻²⁸⁸) argues that the dimeric core structure also will be found in full-length IN. The three catalytic residues, D64, D116, and E152, are visible in at least one monomer of IN⁵²⁻²⁸⁸.

Relationship Between the Catalytic and C-Terminal Domains. The two linking $\alpha 6$ helices of the IN⁵²⁻²⁸⁸ dimer begin in a 2-fold symmetric manner out to T210. A kink in $\alpha 6$ occurs at T210 in one monomer, introducing a 90° rotation of one C-terminal domain and its leading helical stem relative to the other (Fig. 2 *b* and *c*). A previously identified proteolytic cleavage site near T210 suggests that the kink may represent a flexible junction in solution (5). This flexible elbow within $\alpha 6$ may reflect a key functional determinant that permits a dynamic role for each C-terminal domain during the multistep integration process.

In contrast to HIV-1 IN⁵²⁻²⁸⁸, the link between the catalytic and C-terminal domains in the RSV IN structure (32) is comprised of a short, six-residue β -strand that immediately deviates at W213 from the 2-fold symmetry of the core. For SIV IN (28), only one of the four C-terminal domains within the asymmetric unit can be resolved. It is packed against helix $\alpha 6$ within the core domain, and residues 211–220 of the linking sequence do not form a helix. The different orientations of the catalytic core and C-terminal domains among the RSV, SIV, and HIV-1 IN structures further support the notion of a functional flexibility within the linking sequence.

The NMR structure for residues 220–270 of the HIV-1 C-terminal domain is a dimer involving antiparallel, 2-fold related packing of the contiguous $\beta 2$ - $\beta 3$ - $\beta 4$ three-stranded β -sheets against each other (16, 17). Although it differs from all three C-terminal interfaces in the IN⁵²⁻²⁸⁸ crystal structure, the NMR dimer interface most closely resembles IN⁵²⁻²⁸⁸ interface B that involves the $\beta 2$ - $\beta 3$ - $\beta 4$ sheets. However, interface B is mediated by a CHAPS molecule and the sheets in interface B and the NMR structure are packed in opposite orientations. This orientation difference is likely caused by a biologically relevant restriction imposed by having the C-terminal domain linked to the catalytic core domain in IN⁵²⁻²⁸⁸, a restriction not imposed on an isolated C-terminal domain. Although the C-terminal interactions involving adjacent HIV-1 IN⁵²⁻²⁸⁸ dimers determine the crystal packing, they and the dimer interface in the isolated C-terminal structure may represent favorable interactions that facilitate the higher-order complex required for properly spaced, concerted integration into the host DNA. Mutagenesis of residues within the C-terminal domains suggests that higher-order

oligomerization of HIV-1 IN in solution is facilitated by the C-terminal domains (33, 34).

The Viral DNA Binding Platform. A contiguous strip of positive charge extending from the catalytic site along the outside face of the IN⁵²⁻²⁸⁸ dimer includes residue K159, which can cross-link to the adenine of the invariant 3' CA at each viral end (Fig. 3*a*) (35). It continues through residues K186, R187, and K188, and out to residues K211, K215, and K219 of the $\alpha 6$ helix from the paired monomer in the dimer (Fig. 3*a*). This strip of positive potential may provide a platform on which viral *att* site DNA could be stabilized for 3' processing and strand transfer. This putative DNA binding platform involves residues from both monomers within the IN⁵²⁻²⁸⁸ dimer, implying that a viral end cleaved in the active site of one monomer is stabilized by residues from the C terminus of the other monomer. This could explain *in vitro* complementation data in which two inactive IN mutants can be combined to regain IN activity (36, 37). Docking of an 18-bp viral DNA end to IN⁵²⁻²⁸⁸ places the adenine of the conserved viral 3' CA in direct contact with K159, places the active site proximal loop involving residues 186–194 in contact with the major groove of the DNA, and places $\alpha 6$ helix residues K211, K215, and K219 of the other monomer in contact with the DNA backbone phosphates (Fig. 3*b*). In contrast, the structures of two-domain IN from SIV and RSV highlight different putative DNA binding platforms derived from the different spatial arrangements of the C-terminal domain relative to the catalytic core domain. Therefore, the structure of a DNA-bound form of IN will be necessary to distinguish these possibilities.

Residues R263 and K264 in the $\beta 4$ - $\beta 5$ turn of the HIV-1 IN C-terminal domains can be cross-linked to viral DNA 4–6 base pairs, 14–21 Å, from the conserved terminal CA dinucleotide (38–40). This distance is much closer than the 62 Å between the catalytic site and R263 in the IN⁵²⁻²⁸⁸ structure (Fig. 3*b*). The cross-linking data therefore may reflect interactions between viral DNA held by one dimer and the C-terminal domain from an adjacent dimer. This would require two dimers at each viral end or two IN tetramers in a fully active complex. Interestingly, recent cross-linking data suggested an IN octamer as the active complex for concerted integration of both viral ends (40). Alternatively, the connecting $\alpha 6$ helix of one protomer within a dimer could be extended when binding DNA while the connecting $\alpha 6$ helix from the other protomer folds at the flexible elbow (T210), thereby placing R263 \approx 20 Å, or one-half turn of duplex DNA, from the conserved CA

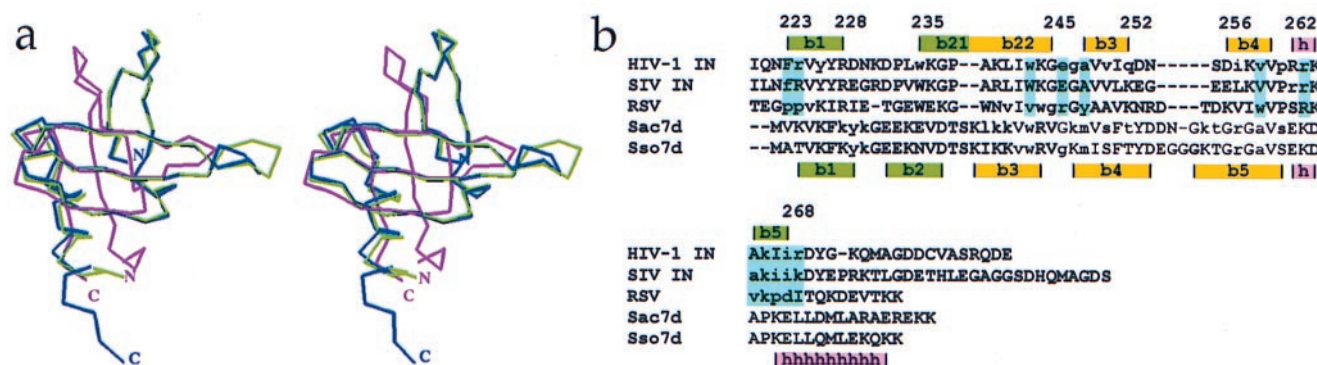


Fig. 6. Comparison of the SH3-like folds from HIV-1 IN, Sac7d, and Sso7d. (a) α -Carbon overlay of the HIV-1 IN C-terminal domain (magenta), Sac7d (green), and Sso7d (blue) structures demonstrates significant structural similarity. (b) Primary sequence alignment of the IN C-terminal domains from HIV-1, SIV, and RSV, and DNA-binding proteins Sac7d and Sso7d based on secondary structure (HIV-1 IN residue numbering). Secondary structural elements are highlighted. Yellow and green denote the β -strands contributing to the β -sandwich structure of the IN C-terminal domains, Sac7d, and Sso7d. Lowercase lettering indicates residues in IN that are involved in protein–protein interactions, and residues in Sac7d and Sso7d that are involved in protein–DNA interactions. Residues highlighted in cyan are involved in protein–protein contacts in at least two of the molecules.

dinucleotide. Extreme $\alpha 6$ flexibility, well beyond what we see for IN (52–288), could allow the C-terminal domain to pack against the catalytic core as seen in the SIV IN structure (28). In any of these models, a flexible elbow in the linking sequence allows the C-terminal domains to help tether the DNA during the integration process.

Interaction of DNA with the C-Terminal Domain. Two structures of DNA-bound to Src homology 3 (SH3)-like folds are known (41–43). The proteins involved, Sso7d and Sac7d, bind in the minor groove of double-stranded DNA in a sequence-independent manner. Hydrophobic groups on the surface of an SH3-fold β -sheet in each protein intercalate into the minor groove of the bound DNA, which widens the groove and sharply kinks the DNA. Although these proteins do not have significant overall sequence homology with the C-terminal domain of HIV-1 IN, alignment of the C-terminal domain crystal structure with those of Sso7d and Sac7d shows that they have similar folds, with rms deviations of 2.2 Å and 1.9 Å, respectively (Fig. 6). The structural similarity is most pronounced at the β -sheet that binds to DNA, which corresponds to the $\beta 2$ - $\beta 3$ - $\beta 4$ sheet that figures prominently in the C-terminal interactions observed in the HIV IN^{52–288} structure (Fig. 5). The hydrophobic surface of this IN β -sheet, and the corresponding ones in Sso7d and Sac7d, includes a conserved W243 that interfaces with CHAPS in the IN structure and with DNA bases in the Sso7d and Sac7d structures. We speculate that the HIV-1 IN $\beta 2$ - $\beta 3$ - $\beta 4$ sheet may bind DNA in a manner analogous to Sso7d and Sac7d.

The diversity and hydrophobic character of the protein–

protein interactions involving the C-terminal domains from HIV-1, RSV (32), and SIV (28) suggest that they are weak and nonspecific. Because of flexibility in the linker between domains, the C-terminal domains can adopt a wide range of orientations relative to the catalytic core, and none of the protein–protein interactions seen in the crystal structures may actually be present in DNA-bound forms of the protein. The interactions do, however, involve residues that are clustered on the $\beta 2$ - $\beta 3$ - $\beta 4$ sheet and on the C-terminal strand $\beta 5$ (Figs. 5 and 6b), suggesting these are binding epitopes that may contribute to DNA binding and IN oligomerization.

HIV-1 IN catalyzes the insertion of the viral cDNA into the human genome and is required for viral replication and pathogenesis (11). As such, IN is a promising target for the design of anti-HIV drugs. The determination of the two-domain HIV-1 IN structure, IN^{52–288}, should prove useful for structure-based efforts to design new IN inhibitors, especially those that may act through perturbation of critical interactions between IN and the viral ends. This can be tested through cocrystallization with DNA and new mutants, experiments that will assist in drug design and will add to our understanding of how IN works.

We thank Harold Varmus with whom we started this effort; Robert Rose, Thomas Anderson, George Robles, Earl Rutenber, and Kimiko Yabe for work performed in the early stages of this project; Aina Cohen and Ashley Deacon at Stanford Synchrotron Radiation Laboratory for assistance with data collection; and Patrick Brown (Stanford University) for sharing his synthetic HIV-1 IN gene. This work was funded by National Institutes of Health Grant GM56531 to R.M.S. and A.D.L.

- Engelman, A., Mizuuchi, K. & Craigie, R. (1991) *Cell* **67**, 1211–1221.
- Johnson, M. S., McClure, M. A., Feng, D. F., Gray, J. & Doolittle, R. F. (1986) *Proc. Natl. Acad. Sci. USA* **83**, 7648–7652.
- Khan, E., Mack, J. P., Katz, R. A., Kulkosky, J. & Skalka, A. M. (1991) *Nucleic Acids Res.* **19**, 851–860.
- Bushman, F. D., Engelman, A., Palmer, I., Wingfield, P. & Craigie, R. (1993) *Proc. Natl. Acad. Sci. USA* **90**, 3428–3432.
- Engelman, A. & Craigie, R. (1992) *J. Virol.* **66**, 6361–6369.
- Leavitt, A. D., Shiue, L. & Varmus, H. E. (1993) *J. Biol. Chem.* **268**, 2113–2119.
- Kulkosky, J., Jones, K. S., Katz, R. A., Mack, J. P. & Skalka, A. M. (1992) *Mol. Cell. Biol.* **12**, 2331–2338.
- van Gent, D. C., Groeneger, A. A. & Plasterk, R. H. (1992) *Proc. Natl. Acad. Sci. USA* **89**, 9598–9602.
- Vincent, K. A., Ellison, V., Chow, S. A. & Brown, P. O. (1993) *J. Virol.* **67**, 425–437.
- Zheng, R., Jenkins, T. & Craigie, R. (1996) *Proc. Natl. Acad. Sci. USA* **93**, 13659–13664.
- Brown, P. (1997) in *Retroviruses*, eds. Coffin, S., Hughes, S. H. & Varmus, H. E. (Cold Spring Harbor Lab. Press, Plainview, NY), pp. 161–203.
- Dyda, F., Hickman, A. B., Jenkins, T. M., Engelman, A., Craigie, R. & Davies, D. R. (1994) *Science* **266**, 1981–1986.
- Jenkins, T. M., Hickman, A. B., Dyda, F., Ghirlando, R., Davies, D. R. & Craigie, R. (1995) *Proc. Natl. Acad. Sci. USA* **92**, 6057–6061.
- Cai, M., Zheng, R., Caffrey, M., Craigie, R., Clore, G. M. & Gronenborn, A. M. (1997) *Nat. Struct. Biol.* **4**, 567–577.
- Cai, M., Huang, Y., Caffrey, M., Zheng, R., Craigie, R., Clore, G. M. & Gronenborn, A. M. (1998) *Protein Sci.* **7**, 2669–2674.
- Eijkelenboom, A. P., Lutzke, R. A., Boelens, R., Plasterk, R. H., Kaptein, R. & Hard, K. (1995) *Nat. Struct. Biol.* **2**, 807–810.
- Lodi, P. J., Ernst, J. A., Kuszewski, J., Hickman, A. B., Engelman, A., Craigie, R., Clore, G. M. & Gronenborn, A. M. (1995) *Biochemistry* **34**, 9826–9833.
- Eijkelenboom, A. P., Sprangers, R., Hard, K., Puras Lutzke, R. A., Plasterk, R. H., Boelens, R. & Kaptein, R. (1999) *Proteins* **36**, 556–564.
- Otwinowski, Z. & Minor, W. (1997) *Methods Enzymol.* **276**, 307–326.
- Brunger, A. T., Adams, P. D., Clore, G. M., Delano, W. L., Gros, P., Grosse-Kunstleve, R. W., Jiang, J.-S., Kuszewski, J., Nilges, M., Pannu, N. S., et al. (1998) *Acta Crystallogr. D* **54**, 905–921.
- Goldgur, Y., Dyda, F., Hickman, A. B., Jenkins, T. M., Craigie, R. & Davies, D. R. (1998) *Proc. Natl. Acad. Sci. USA* **95**, 9150–9154.
- Chambers, J. L. & Stroud, R. M. (1977) *Acta Crystallogr. B* **33**, 1824–1837.
- Sack, J. S. (1988) *J. Mol. Graphics* **6**, 224–225.
- Kissinger, C. R., Gehlhaar, D. K. & Fogel, D. B. (1999) *Acta Crystallogr. D* **55**, 484–491.
- Aiken, C., Konner, J., Landau, N. R., Lenburg, M. E. & Trono, D. (1994) *Cell* **76**, 853–864.
- Maignan, S., Guilloteau, J. P., Zhou-Liu, Q., Clement-Mella, C. & Mikol, V. (1998) *J. Mol. Biol.* **282**, 359–368.
- Greenwald, J., Le, V., Butler, S. L., Bushman, F. & Choe, S. (1999) *Biochemistry* **38**, 8892–8898.
- Chen, Z., Yan, Y., Munshi, S., Li, Y., Zugay-Murphy, J., Xu, B., Witmer, M., Felock, P., Wolfe, A., Sardana, V., et al. (2000) *J. Mol. Biol.* **296**, 521–533.
- Bujacz, G., Jaskolski, M., Alexandratos, J., Wlodawer, A., Merkel, G., Katz, R. A. & Skalka, A. M. (1995) *J. Mol. Biol.* **253**, 333–346.
- Stroud, R. M. & Fauman, E. B. (1995) *Protein Sci.* **4**, 2392–2404.
- Bujacz, G., Alexandratos, J., Qing, Z. L., Clément-Mella, C. & Wlodawer, A. (1996) *FEBS Lett.* **398**, 175–178.
- Yang, Z. N., Mueser, T. C., Bushman, F. D. & Hyde, C. C. (2000) *J. Mol. Biol.* **296**, 535–548.
- Paras Lutzke, R. A. & Plasterk, R. H. A. (1998) *J. Virol.* **72**, 4841–4848.
- Jenkins, T. M., Engelman, A., Ghirlando, R. & Craigie, R. (1996) *J. Biol. Chem.* **271**, 7712–7718.
- Jenkins, T. M., Esposito, D., Engelman, A. & Craigie, R. (1997) *EMBO J.* **16**, 6849–6859.
- van Gent, D. C., Vink, C., Groeneger, A. A. & Plasterk, R. H. (1993) *EMBO J.* **12**, 3261–3267.
- Engelman, A., Bushman, F. D. & Craigie, R. (1993) *EMBO J.* **12**, 3269–3275.
- Esposito, D. & Craigie, R. (1998) *EMBO J.* **17**, 5832–5843.
- Heuer, T. S. & Brown, P. O. (1997) *Biochemistry* **36**, 10655–10665.
- Heuer, T. S. & Brown, P. O. (1998) *Biochemistry* **37**, 6667–6678.
- Robinson, H., Gao, Y. G., McCrary, B. S., Edmondson, S. P., Shriver, J. W. & Wang, A. H. (1998) *Nature (London)* **392**, 202–205.
- Krueger, J. K., McCrary, B. S., Wang, A. H., Shriver, J. W., Trewhella, J. & Edmondson, S. P. (1999) *Biochemistry* **38**, 10247–10255.
- Gao, Y. G., Su, S. Y., Robinson, H., Padmanabhan, S., Lim, L., McCrary, B. S., Edmondson, S. P., Shriver, J. W. & Wang, A. H. (1998) *Nat. Struct. Biol.* **5**, 782–786.
- Kraulis, P. J. (1991) *J. Appl. Crystallogr.* **24**, 946–950.
- Merritt, E. A. & Murphy, M. E. P. (1994) *Acta Crystallogr. D* **50**, 869–873.
- Ferrin, T. E., Huang, C. C., Jarvis, L. E. & Langridge, R. (1988) *J. Mol. Graphics* **6**, 13–27.
- Nicholls, A., Sharp, K. A. & Honig, B. (1991) *Proteins* **11**, 281–296.
- CCP4 (1994) *Acta Crystallogr. D* **50**, 760–763.